WSPH AND ISPH CALCULATIONS OF A COUNTER-ROTATING VORTEX DIPOLE.

L. M. González, J.M. Sánchez, F. Macià, D. Duque, J. Gómez-Goñi
Naval Arquitecture School
Universidad Politécnica de Madrid
Madrid, Spain
leo.gonzalez@upm.es

M.A. Rodríguez-Perez
Cellular Materials Group (CellMat), Condensed Matter Physics Department
Universidad de Valladolid
Valladolid, Spain

Abstract—**Viscosity and vorticity are magnitudes playing an important role in many engineering physical phenomena such as: boundary layer separation, transition flows, shear flows, etc., demonstrating the importance of the vortical viscous flows commonly used among the SPH community.**

The simulation presented here, describes the physics of a pair of counter-rotating vortices in which the strain field felt by each vortex is due to the other one. Different from the evolution of a single isolated vortex, in this case each vortex is subjected to an external stationary strain field generated by the other, making the streamlines deform elliptically. To avoid the boundary influence, a large computational domain has been used ensuring insignificant effect of the boundary conditions on the solution. The performance of the most commonly used viscous models in simulating laminar flows, Takeda's(TVT), Morris'(MVT) and Monaghan-Cleary's(MCGVT) has been discussed comparing their results. These viscous models have been used under two different compressibility hypotheses.

Two cases have been numerically analyzed in this presentation. In the first case, a 2D system of two counter-rotating Lamb-Oseen vortices is considered. At first, the system goes through a rapid relaxation process in which both vortices equilibrate each other. This quasi-steady state is obtained after the relaxation phase is advected at a constant speed and slowly evolves owing to viscous diffusion. The results of the different Lamb-Oseen numerical solutions have been validated with good agreement by comparison with the numerical results of a finite element code (ADFC) solution. A second case, somewhat more complex than the previous one, is a 3D Batchelor vortex dipole obtained by adding an axial flow to the system of the first case. The Batchelor vortex model considered here is a classical option normally used to model the structure of trailing vortices in the far-wake of an aircraft.

I. Introduction and Motivation

Modeling low Reynolds number vortical viscous flows does not present excessive difficulties for industrial focused CFD methods like finite element method (FEM). Nevertheless, these methods encounter difficulties when dealing with problems such as highly distorted free surface flows, where SPH is probably the first option. Laminar solutions of the incompressible Navier-Stokes and continuity equations, describing the evolution of vortex laminar systems, have been efficiently obtained by both weakly compressible SPH (WSPH) and incompressible SPH (ISPH) methods. Several examples of simulation of isolated vortices [1]–[3] and periodic Taylor-Green flows [4], [5] can be found in the literature. The motivation for the present study is to extend the SPH method to model the interaction of the counter-rotating vortices created at the far wake of an aircraft, an interesting aeronautical application. Aircraft in flight leave behind large-scale swirling flows (vortices), which can represent a significant hazard to following aircraft, and therefore are of great importance for practical applications concerning safety and capacity of air transport, see [6].

Trailing vortices are a natural byproduct of airplanes, and other vehicles, with finite-span lifting wings. Lift is generated by pressure differences on the upper and lower surfaces of the wings. These pressure differences lead to the creation of vortices that trail behind the airplane and persist well downstream of the vehicle. The vortices (sometimes referred to as wake vortices, or wake turbulence) are characterized by a rotational flow field, analogous to a set of tornados turned sideways with their cores aligned in the flight-path direction. The circulation strength of the vortices is proportional to the total lift (which supports the airplane weight), and inversely proportional to the vortex span (which depends on the geometric wing span and the distribution of lift along the wings) and the airplane speed. Practical interest in trailing vortices is motivated by their potential impact to following airplanes that might encounter them. As an airplane flies into the vortices of another aircraft it can experience a significant upset. This can result in the rapid rolling of the airplane due to the rotational flow, and/or a drop in the airplanes altitude. Depending on the severity of the upset and the proximity to the ground, a vortex encounter can be a safety hazard. This is a critical issue for airplanes when arriving to and departing from airports. In order to avoid unsafe encounters near the ground, regulators have imposed airplane separation requirements for operations

Fig. 1. Aircraft vortex scheme.

under instrument flight rules. The separations allow time for the vortices to be carried away from the flight path by the self induction of the rotational flow or by atmospheric currents. The separation time also allows for some amount of natural decay or breakup to occur. These separations have proven to be safe; however, they contribute to airport delays and reductions in airport capacity. Thus, the ability to minimize or destroy the vortices would be of significant benefit to air-traffic capacity in the airport terminal area. Such control could be exploited to improve airport capacity, while maintaining the safety of the current air-traffic management system. The basic physics of the breakup scheme are examined using a simplified model for the vortex system.

The aircraft wake model can be efficiently described by an external vortex pair modeling the wing tip vortices and an internal vortex pair rotating in the opposite direction modeling the vortices generated by the fuselage and the horizontal tail, see Figure 1. This creating a pair of co-rotating vortices at each side of the aircraft. The evolution of this co-rotating couple is very unstable merging quickly into a single vortex on each side. Consequently the final scenario is the presence of two counter-rotating vortices coming from each wing.

Our numerical study considers first a 2D system of two counter-rotating Lamb-Oseen vortices. The main differences of this problem with the Taylor-Green vortex evolution are:

- There is no analytical solution for this flow.
- No periodic boundary conditions are used.
- The vortex evolution does not converge towards a stationary solution, meaning that particles are constantly moving.

A second problem that is also considered is a 3D Batchelor vortex dipole obtained by adding an axial flow to the first problem. The presence of an axial flow does not modify the two-dimensional equilibrium solution because the dynamics of the axial velocity is decoupled from the dynamics of other velocity components and can be treated separately. Thus, if we consider an axial flow velocity field proportional to the axial vorticity, we can automatically form a complete 3D solution. The Batchelor vortex here considered is a classical option normally used to model the structure of trailing vortices in the far-wake of an aircraft [7].

The simulation is initiated with two counter-rotating Gaussian vortices without axial flow of core radius a, circulation Γ, and separated by a distance b. In this evolutionary process there is first a rapid relaxation phase during which the vortices equilibrate with each other [8]. This quasi-steady state is obtained after the relaxation process is advected at a constant speed and slowly evolves owing to viscous diffusion. To model this problem, both a weakly compressible code and an incompressible code have been developed and their advantages and drawbacks have been studied comparing their performance.

Traditionally incompressible flows have been simulated in the SPH context using a weakly compressible approach, hereafter referred to as WCSPH. In this approximation the pressure depends on the density through an algebraic thermodynamic equation and the density in turn, is transported according to the compressible mass conservation equation. Three important features of this approach are:

- A very small time step is required to maintain the numerical stability of the simulation due to the fact that this time step is calculated with the sound speed which is at least 10 times higher than the maximum of velocity.
- The pressure is based on density values, this provokes that small density fluctuations cause significant pressure variations with large errors when compared with the reference solution including the possibility of causing tensile [9] or numerical instabilities.
- There is no need to choose adequate equations of state and Mach numbers and its corresponding parameters.

The evolution of the incompressible SPH meshless methods hereafter referred to as ICSPH, starts in [10] where Koshizuka et al. force the incompressibility, keeping the particle number density constant. The continuity equation is written in the form $\frac{d\rho}{dt} = 0$. When the particle number density $n_i(t) = \sum_j W(r_j - r_i)$ differs from the goal, the constant initial value n_0, the pressure is corrected in order to meet the goal and the particle density is recalculated. This pressure correction is applied to every particle iteratively so as to satisfy the proposed continuity equation. In a second paper [11] Koshizuka et al. solved the Poisson equation, when the right hand side represents the deviation of the particle number density from the initial constant value. In this case, the corresponding linear system is solved by an Incomplete Cholesky Conjugate Gradient method. A seminal paper in the incompressible context is due to Cummins [2], where a fractional step method is used. In it, the intermediate velocity is projected onto a divergence-free space by solving a Poisson equation derived from an approximate pressure projection. A Jacobi Conjugate Gradient method was used to solve this linear system. In [5], a kinematic constrain was imposed by Ellero et al. to force the volume of fluid particles to be constant. This is performed by the calculation of certain Lagrange multipliers through the iterative SHAKE algorithm. Another important paper comes from Hu et al. [4] where a fractional step method is developed to enforce both the zero-density-variation condition and the velocity-divergence-

free condition at each full time step. A slight variant with particle shifting of Hu's method was proposed by Xu et al. in [12]. In Lee et al. [13] a divergence free velocity field is obtained by a fractional step method calculating a stable local pressure in the dam break problem, it is remarkable that no preconditioning was used to solve the linear system. An interesting difference can be found between the last paper and the one presented by Khayyer et al. [14] where a matrix correction is applied to the gradient calculations to obtain an improved SPH momentum conservation formulation. Finally, in Raffiee et al. [15] an explicit but iterative formulation for the Poisson equation was presented to force the mass conservation.

II. Computational methods

As has been mentioned, our goal is to simulate newtonian and incompressible viscous flow in laminar regime. In the continuous formulation, these flows are well described by the Navier-Stokes equations:

$$\nabla \cdot \mathbf{v} = 0 \tag{1}$$

$$\rho \frac{d\,\mathbf{v}}{dt} = -\nabla p + \mu \nabla^2 \mathbf{v} \tag{2}$$

in which p is the pressure, ρ the density, $\mathbf{v}$ the velocity and t is the time.

The equation (1) and the pressure term in the equation (2) play a combined role in which the pressure acts as a Lagrange multiplier that produce a zero divergence velocity field. If the incompressibility condition is imposed, either a penalty formulation or a pressure Poisson equation must be solved to calculate the pressure values increasing the computational work substantially. In the WCSPH context this hypothesis is relaxed assuming a weakly compressible fluid with a large sound speed, where the equation (1) is replaced by

$$\frac{d\rho}{dt} = -\rho \nabla \cdot \mathbf{v} \tag{3}$$

and an equation of state $p = p(\rho)$ must be added to the system. Finally if a Lagrangian description of the fluid is assumed, the fluid particles move according to the kinematic law:

$$\frac{d\mathbf{r}}{dt} = \mathbf{v} \tag{4}$$

The WCSPH equations implemented in this work are similar to the ones used in [3]. The kernel will be a renormalized Gaussian kernel with a support of $3h$ and $h = kdx$ where dx is the typical initial separation among particles and $k \geq 1.33$ is a free parameter that quantifies the neighbor particle influence.

The integration in time has been performed using a Leapfrog second order scheme. The selection of the time step has been based on the viscous diffusion, convective, acceleration, and sound waves propagation terms. The CFL factor used was 1/8 using h as a reference length. No special initialization or stabilization technique has been used.

The ISPH formulation used follows the scheme described in [13]. Due to the symmetric structure of the coefficient matrix that represents the Laplace operator, the Poisson problem was solved by a Conjugate Gradient (CG) method. Two different preconditioners were used for this system, the most costly computationally was the incomplete Cholesky (IC) where the number of iterations to obtain a residual $\sim O(10^{-13})$ was less than 40 when the Reynolds number $Re = 100$. A second possibility using a Jacobi diagonal preconditioner was computationally cheaper but the number of iterations increased by an order of magnitude. Finally, without any preconditioner, the number of iterations was similar to the Jacobi case. Taking into account that the time used in the preconditioner stage is considerably larger than the computational time consumed by the CG iterations, it was decided not to use any preconditioner in our calculations. The computational domain was selected large enough to make the solution independent of the boundary influence. Different computational domains were tested until the solution showed no influence. The boundary condition used for the velocity was the no-slip condition. This was implemented by three rows of fixed fluid (dummy) particles that were treated as common fluid particles with the only difference that they are not displaced in time. The boundary condition used for the pressure in the Poisson problem was Neumann homogeneous type $\partial p/\partial n = 0$. Differing from the strategy used in [2], it can be shown that implementation of this pressure boundary condition is unnecessary in the homogeneous case. Indeed, starting with the approximation:

$$\nabla^2 p(\mathbf{r}) \cong \int_{\Omega} \nabla^2 \mathbf{p}(\mathbf{r}^{'}) \mathbf{W}(\mathbf{r}' - \mathbf{r}) \mathbf{d\Omega} \tag{5}$$

Integrating by parts and applying the Gauss' theorem:

$$\nabla^2 p(\mathbf{r}) \cong -\int_{\Omega} \nabla \mathbf{p}(\mathbf{r}^{'}) \nabla \mathbf{W}(\mathbf{r}^{'} - \mathbf{r}) \mathbf{d\Omega} + \int_{\Gamma} \frac{\partial \mathbf{p}(\mathbf{r}^{'})}{\partial \mathbf{n}} \mathbf{W}(\mathbf{r}^{'} - \mathbf{r}) \mathbf{d\Gamma} \tag{6}$$

Applying the homogeneous boundary condition, the second integral vanishes. Using the following approximations:

$$p(\mathbf{r}^{'}) - \mathbf{p}(\mathbf{r}) \cdot (\mathbf{r}^{'} - \mathbf{r}) = \nabla \mathbf{p}(\mathbf{r}) (\mathbf{r}^{'} - \mathbf{r})^{\mathbf{2}} \tag{7}$$

we have

$$\nabla^2 p(\mathbf{r}) \cong -\int_{\Omega} \frac{\mathbf{p}(\mathbf{r}^{'}) - \mathbf{p}(\mathbf{r}^{'}) \cdot (\mathbf{r}^{'} - \mathbf{r}^{'})}{(\mathbf{r}^{'} - \mathbf{r}^{'})^{\mathbf{2}}} \nabla \mathbf{W}(\mathbf{r}^{'} - \mathbf{r}) \mathbf{d\Omega} \tag{8}$$

The equivalent SPH discretization according to [2], [13] should be:

$$\nabla^2 p(\mathbf{r_a}) \cong \sum_{\mathbf{b}} \frac{\mathbf{2m_b}}{\rho_{\mathbf{b}}} \frac{\mathbf{p_{ab}} \mathbf{r_{ab}} \cdot \nabla \mathbf{W}(\mathbf{r_{ab}})}{\mathbf{r_{ab}}^{\mathbf{2}}} \tag{9}$$

Demonstrating that imposing homogeneous boundary conditions is equivalent to the vanishing of the boundary integral and there is no need of fictitious particles to impose the condition. However, it is important to impose the pressure value on a certain fluid particle because the Poisson problem is not completely determined. In our case this was done imposing $p = 0$ for the particle that initially is at the center of the domain.

III. VISCOSITY MODELS

A. General

In our analysis we have selected three different SPH implementations of the real viscous terms in the Navier-Stokes linear momentum equation that are very representative of three different stages in the simulation of SPH physical viscosities. A complete description of the history, properties and evolution of the viscous models can be found in [3], here we will limit ourselves to present the mathematical expressions of the models considered in this work.

B. Monaghan-Cleary-Gingold's

The expression used for the (MCGVT) is

$$\mathbf{\Pi}_a^{MCGVT} = -\frac{8\mu}{\rho_a}\sum_b \frac{m_b}{\rho_b}\frac{\mathbf{v}_{ab}\cdot\mathbf{r}_{ab}}{r_{ab}^2}\nabla_a W_{ab} \qquad (10)$$

where ρ_a and ρ_b are the density of particles a and b, $\mathbf{r}_{ab} = \mathbf{r}_a - \mathbf{r}_b$ and W_{ab} is the value of the kernel for particle a evaluated at particle b, ∇_a denotes the gradient of the kernel taken with respect to the coordinates of particle a.

C. Morris et al.

Morris et al. [16] estimated the shear viscosity term in the linear momentum Navier Stokes equation for incompressible flow as:

$$\mathbf{\Pi}_a^{MVT} = \sum_b \frac{m_b}{\rho_a\rho_b}\left(\mu_a+\mu_b\right)\mathbf{v}_{ab}\frac{\mathbf{r}_{ab}\cdot\nabla_a W_{ab}}{r_{ab}^2} \qquad (11)$$

It conserves the linear momentum while the angular momentum is not conserved, a desirable feature of relative importance in low Reynolds number flows and in many industrial fluid problems [1].

D. Takeda et al.

Takeda et al. [17] considered the linear momentum equation relative to a compressible stokesian fluid

$$\frac{d\mathbf{v}}{dt} = -\frac{1}{\rho}\nabla p + \frac{\mu}{\rho}\left(\nabla^2\mathbf{v} + \frac{1}{3}\nabla(\nabla\cdot\mathbf{v})\right) \qquad (12)$$

and found their SPH viscous term (TVT) by differentiating the SPH interpolant twice, followed by a subsequent process of anti-symmetrization to recover the conservation of the linear momentum.

Assuming that the kernel is a function of r_{ab}, we get the viscous term

$$\begin{aligned}\mathbf{\Pi}_a^{TVT} = \frac{-\mu}{\rho_a}\sum_b \frac{m_b}{\rho_b}\Bigg\{&\left(r_{ab}\frac{\partial}{\partial r_{ab}}\left(\frac{1}{r_{ab}}\frac{\partial W_{ab}}{\partial r_{ab}}\right)+\right.\\ &\left.+\frac{2}{r_{ab}}\frac{\partial W_{ab}}{\partial r_{ab}}\right)\mathbf{v}_{ab} + \frac{1}{3}\left[\left(\frac{1}{r_{ab}}\frac{\partial W_{ab}}{\partial r_{ab}}\right)\mathbf{v}_{ab}+\right.\\ &\left.+\frac{\partial}{\partial r_{ab}}\left(\frac{1}{r_{ab}}\frac{\partial W_{ab}}{\partial r_{ab}}\right)\frac{\mathbf{r}_{ab}\cdot\mathbf{v}_{ab}}{r_{ab}}\mathbf{r}_{ab}\right]\Bigg\}\end{aligned} \qquad (13)$$

where we have split each term of the sum into one term linked to the shear viscosity, the one parallel to $\mathbf{v}_{ab}$ that explicitly reproduces in the discrete formulation the role played by the Laplacian in the continuum, and a second one representing the compressible viscosity.

IV. 2D LAMB-OSEEN VORTEX DIPOLE.

From the different models available in the literature to model vortex dynamics, the Lamb-Oseen viscous vortex model was selected based on its relevance as the most frequently used model to simulate the evolution and stability of aircraft wakes. The vortices are initially placed along the X axis at $x = \pm x_0$. The initial condition for the components of the velocity field $\mathbf{v^0} = (\mathbf{v_x^0}, \mathbf{v_y^0})$ is given by the equations:

$$v_x^0 = qy\left\{\frac{1-e^{-r_-^2}}{r_-^2} + \frac{1-e^{-r_+^2}}{r_+^2}\right\} \qquad (14)$$

$$v_y^0 = q\left\{(x-x_0)\frac{1-e^{-r_-^2}}{r_-^2} - (x+x_0)\frac{1-e^{-r_+^2}}{r_+^2}\right\} \qquad (15)$$

where q is the swirl parameter, equal to 0.5 in this work, r_+ is the distance from the fluid particle at (x, y) to the point $(x_0, 0)$ and r_- is the distance from the fluid particle at (x, y) to the point $(-x_0, 0)$. The circulation of each vortex is $\Gamma = 2\pi q$. The Reynolds number Re characterizing the viscous regime will be defined as $Re = \Gamma/\nu$ where ν is the kinematic viscosity.

In the initial configuration, a number of particles of equal mass were placed on concentric rings in the circular domain, starting with one particle at the center. These rings were equally spaced with spacing $\triangle p = R/nr$, where $R = 20$ is the radius of the domain. To ensure the insignificant influence of the Dirichlet boundary conditions used in the external boundary, the value of R was increased until the results were independent of this parameter. The particles were equally spaced around the rings and the number of particles placed at the ring of radius r was $np(r) = nint(2\pi r/\triangle p)$, where $nint$ means the nearest integer number. In these simulations, the last three rows of boundary fluid particles are used to force the boundary condition.

V. WCSPH RESULTS

Two different number of rings have been used in these simulations $nr = 526$ and $nr = 590$, where the second one involves more than a million particles. The ratio h/dx was fixed to 1.33. The equation of state used for this case was:

$$p = \frac{\rho_0 c_s^2}{\gamma}\left[\left(\frac{\rho}{\rho_0}\right)^\gamma - 1\right] \qquad (16)$$

where ρ_0 is the reference density fixed in 1.0, c_s is the numerical sound speed and $\gamma = 7$. Figure 2 shows a reference numerical solution obtained by FEM with the code ADFC at $t = 14s$ with the Reynolds number $Re = 100$. This solution has been obtained in a circular domain of radius $R = 30$, with two different mesh sizes, $h = 0.05$ for the inner part ($r \leq 5$) where all the dominant physics takes place and $h = 2$ for the outer domain ($r > 5$). Comparing the density of the degrees of freedom of the system D_g, the number of nodes per unit surface in the inner part of the FEM domain and the number of particles per unit surface with 590 rings in the WCSPH version, we can estimate that $D_g(FEM) = 1856$ nodes/m^2 and $D_g(WCSPH) = 882$ particles/m^2. The WCSPH solution

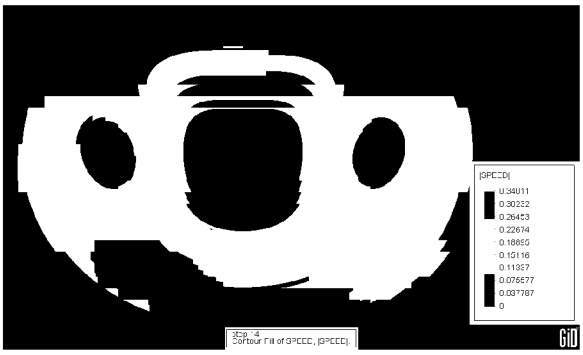

Fig. 2. Snapshot of the velocity magnitude at time $t = 14s$ calculated by FEM.

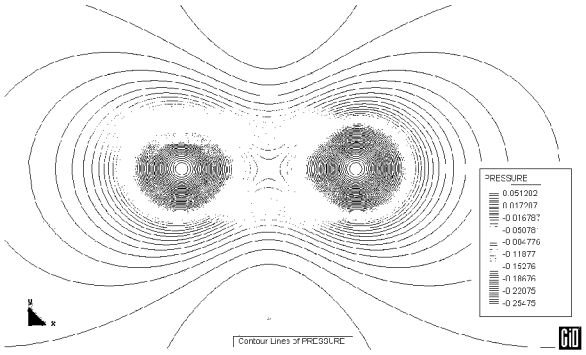

Fig. 4. Pressure field at $t = 1$ for $Re = 100$ calculated by the ADFC-FEM code

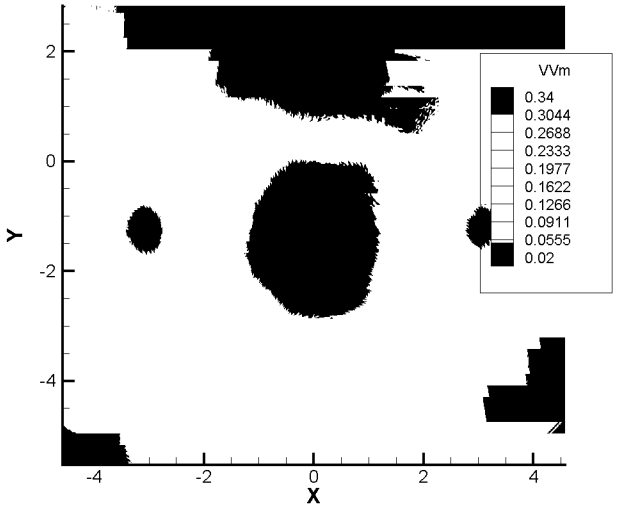

Fig. 3. Snapshot of the velocity magnitude at time $t = 14s$ calculated by WCSPH(TVT).$nr = 526$ and $h = 1.33dx$

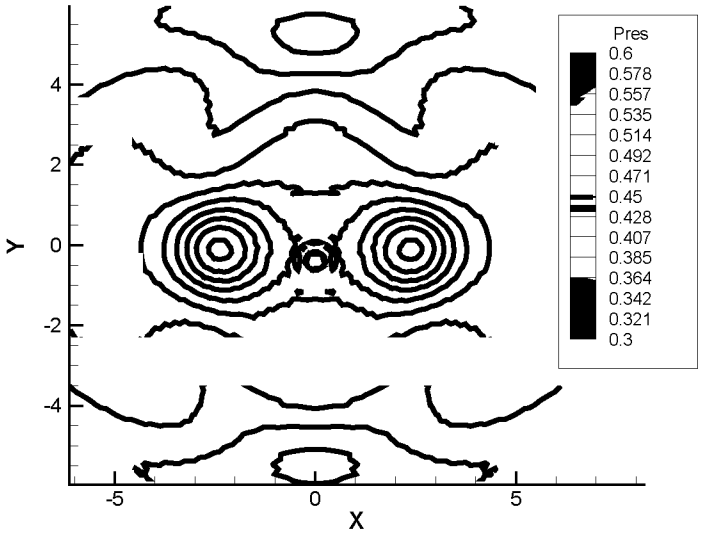

Fig. 5. Pressure field at $t = 1$ for $Re = 100$ calculated by the WCSPH code.

is displayed in Figure 3, where apart from some color scale discrepancies, the qualitative similarity can be appreciated.

In order to quantify the diffusion process produced by this vortex couple, the time evolution of the maximum of the velocity has been plotted using the three different viscous models. It is clear in Figure 8(a) that none of the viscous models captures the evolution of the maximum of the velocity and large oscillations can be appreciated in the maximum velocity evolution curves. Although the aspect of the evolution of the vortices seems reasonable, the diffusion process could be much improved. As it is also evident in this paper, the WCSPH solution is not accurate enough when compared with the ADFC-FEM solution regarding the pressure field. See in Figures 4 and 5 the significant difference in the constant pressure lines between both models.

The evolution of the y-coordinate of the velocity centroid y_V has been discussed as a final measure of the discrepancy between the WCSPH and the ADFC-FEM numerical solutions. This y_V is calculated according to the law:

$$y_V = \frac{\sum_{i=1}^{N} y_i |\mathbf{v_i}|}{\sum_{i=1}^{N} |\mathbf{v_i}|} \tag{17}$$

In Figure 6 it can be appreciated that the evolution of the value of y_V differs significantly from the one shown by the FEM code. According to these results, it was decided to move from the weakly compressible to the incompressible hypothesis.

VI. ISPH RESULTS

The configuration used in this case was identical to the one implemented in the WCSPH test. As it was mentioned in the introduction, the need to solve a Poisson equation at

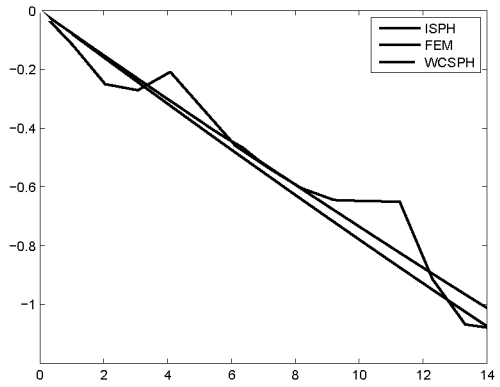

Fig. 6. Evolution of y-coordinate of the velocity center calculated with the MCGVT.

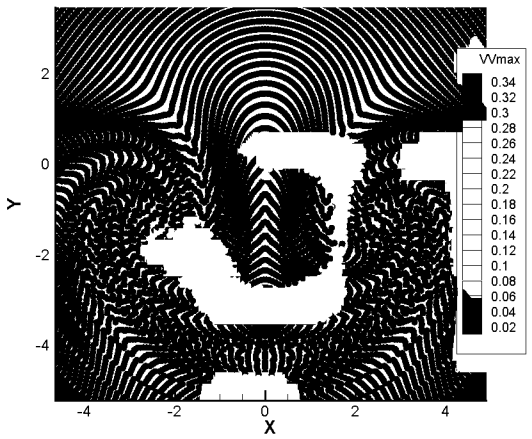

Fig. 7. Snapshot of the velocity magnitude at time $t = 14s$ calculated by ISPH(TVT).$nr = 186$ and $h = 1.8dx$

each time step plus the storage of the corresponding matrix, limit the number of rings in the simulations that have a computational cost similar to the WCSPH. In order to obtain a converged solution, two different number of rings have been used in these simulations $nr = 126$ and $nr = 186$. In this case the comparison of the node density in the inner part of the FEM domain and the particle density with 186 rings in the ISPH version, can be estimated as $D_g(FEM) = 1856$ nodes/m^2 and $D_g(ISPH) = 90$ particles/m^2. Three different ratios $h/dx = 1.33, 1.5, 1.8$ have also been considered. In our code a projection scheme similar to the one used by [13] has been implemented, and the Poisson problem has been solved by an iterative CG method without any preconditioning. The convergence tolerance for the linear solver has been fixed in 10^{-13} and the average number of iterations to meet this tolerance was approximately 550. Comparing Figure 2 and the solution obtained by ISPH displayed in Figure 7 it can be appreciated the qualitative similarity regardless the evident decrease of the number of particles involved in the calculation and some color scale details.

The time evolution of the maximum of the velocity will also be used to quantify the diffusion process produced by the vortex couple. The ISPH graphs of the maximum velocity vs. time for the three different viscous models are represented in Figure 8(b) for $nr = 126$, where the good agreement of the MCGVT and the MVT curves when compared to the FEM reference curve is evident, in contrast with the behavior of the corresponding WCSPH graphs. The ISPH graph corresponding to the TVT viscous model for $nr = 126$, shows initially a good performance that is followed by a large oscillation. As it will be shown next, all these discrepancies disappear increasing the number of rings and the interpolation ratio h/dx.

The difference between the FEM evolution curves and the ones obtained by the MCGVT and the MVT can be explained in terms of lack of accuracy in the interpolation due to the number of particles employed. In fact, if the ratio h/dx is increased, the curves approximate the reference result for the three viscous models studied in this work. For simplicity only

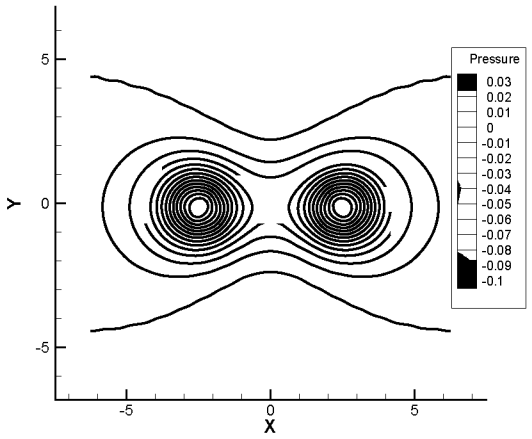

Fig. 10. Pressure field at $t = 1$ for $Re = 100$ calculated by the ISPH code.

the MCGVT and TVT have been represented, see Figures 9(a) and 9(b). This means that the interpolation properties of the numerical discretization play a crucial role in the diffusion process. An interesting result presented in this paper appears when the ISPH calculates the pressure field at time $t = 1s$. In Figure 10 the good agreement in the constant pressure lines between this model and the reference solution shown in Figure 4 can be appreciated. It should be remarked that a smoother solution in the pressure field is obtained by the ISPH, particularly when this solution is compared with the WCSPH one.

Finally the evolution of the y-coordinate of the velocity centroid y_V is also compared both with the FEM reference solution and the WCSPH solution. In Figure 6 can be appreciated that the evolution of the value of y_V is similar to the one represented by the FEM code.

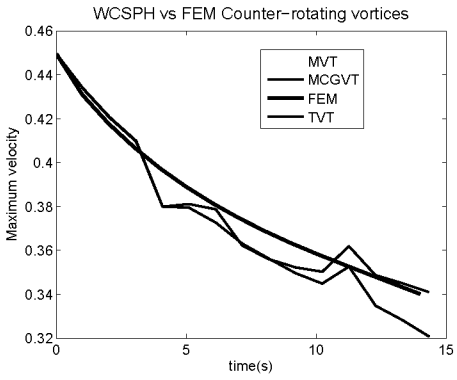

(a) WCSPH

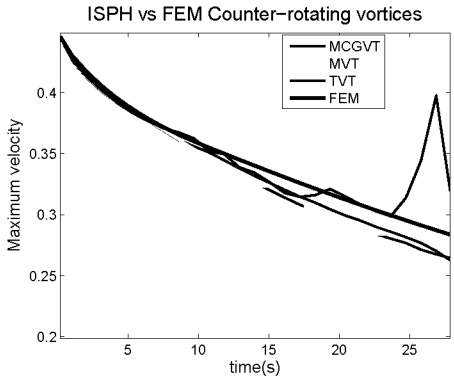

(b) ISPH

Fig. 8. Comparison of the evolution of the maximum of the velocity performed by the WCSPH(nr=526) and the ISPH(nr=126) and different viscosity models.

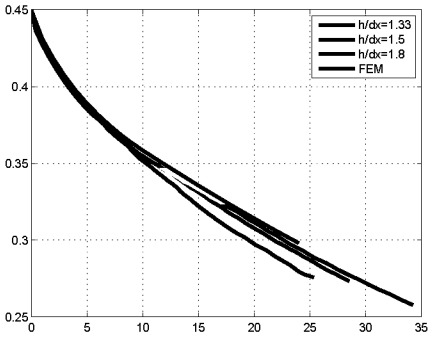

(a) MCGVT

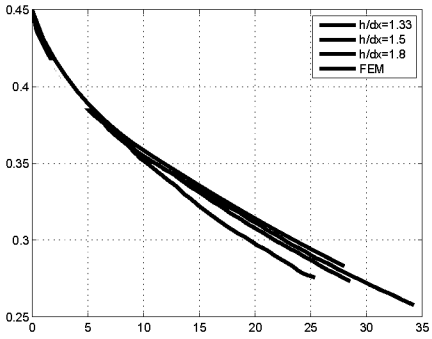

(b) TVT

Fig. 9. Comparison of the evolution of the velocity maximum using the incompressible version. Both, the MCGVT and TVT model have been calculated with nr=126, when the ratio h/dx is increased.

VII. 3D Batchelor vortex

In order to achieve a more realistic model of the structure of trailing vortices in the aircraft far-wake, a more complex 3D Batchelor vortex dipole is also simulated adding an axial flow to the 2D case and increasing notably the Reynolds number. The Batchelor vortex model considered here is a classical option that adds to the velocity field represented by the equations (14) and (15), a third velocity component v_z^0 initialized as:

$$v_z^0 = W(e^{-r_-^2} + e^{-r_+^2}) \tag{18}$$

where W is the axial core velocity parameter.

Under the hypothesis that none of the fluid variables depends on the z coordinate, the two-dimensional evolution of the axial flow is completely decoupled from the dynamics of the other velocity components and can be treated separately. This axial component satisfies the same advection diffusion equation as the axial vorticity.

In Figure 11 the axial component of the flow is shown at a moderate Reynolds number $Re = 5000$

VIII. Conclusions

Two different SPH versions, weakly compressible and fully incompressible, have been used to simulate the physics involved in the interaction of two counter-rotating vortices. For each version, three different viscosity models have been considered. Different from the calculations performed in the isolated Lamb-Oseen vortex in [3], this case takes place in a fully 2D velocity field, which transforms the diffusion process into a more complex one. Comparing a numerical reference solution obtained by FEM with the SPH solutions, pressure and velocity plots have been shown and quantitative results of the evolution of the maximum velocity and the vertical coordinate of the velocity center have been superposed. A significant improvement has been obtained when the ISPH version is used compared with the WCSPH in all the magnitudes plotted. Finally, to achieve a more realistic model of the structure of the trailing vortices that appear in an aircraft wake, an axial velocity component has been added to the ISPH version showing that the velocity fields calculated are suitable to be used in vortex stability calculations.